Dense arrays of short streamers for ultrahigh-resolution 3D seismic imaging

Brian N. Brookshire, Jr.[1], Craig Lippus[2], Abby Parish[1], Brandon Mattox[1], and Allen Burks[1]

Abstract

Ultrahigh-resolution 3D (UHR3D) seismic systems employing a dense array of short streamers represent a significant advancement in the field of marine seismic data acquisition and are an appropriate choice for many near-surface survey applications. Data comparisons between conventional 3D, reprocessed 3D, high-resolution 2D, and UHR3D seismic data illustrate the benefits of a UHR3D acquisition strategy. Results from a recent study of seeps imaged in the Gulf of Mexico (GoM) suggest that UHR3D data can serve as a comprehensive data source for some near-surface geophysical characterizations, satisfying many of the needs often addressed by integrating multiple separate types of survey data.

Introduction

Particularly when times are tough for the oil industry, economists like to point out that what the end user wants/needs is not necessarily something that is better, but something that more completely meets the end user's existing needs in a cost-effective way. This bears heavily on the type of offering(s) that an offshore service company makes. Some of the Goliaths in the industry are asymptotically approaching completeness by sheer size and scope of subsidiary and affiliate companies. In the case of marine seismic acquisition, the majority of major geophysical contractors are increasing value to the customer by going bigger — bigger ships, more streamers, and gigantic production rates.

There is, however, another end of the spectrum wherein a niche group of geophysical contractors is bringing value by offering a product that is not bigger but is fit for purpose and, by virtue of fidelity and resolution, gives a more complete picture of a specific type of target, such as shallow hazards. Multiple products available on the market today support this subdiscipline of seismic acquisition (Hill et al., 2015). For the purposes of this article, the specific cases that we present are based on the use of a P-Cable ultrahigh-resolution 3D (UHR3D) seismic system.

UHR3D systems have been employed and vetted in the commercial sector over the past five years in applications including fault investigations around nuclear power plants off the coast of California (Kluesner and Brothers, 2016); shallow exploration in the Barents Sea (Eriksen et al., 2014); and geohazard investigations in the Gulf of Mexico (GoM) (Brookshire et al., 2015). In the academic sector, UHR3D systems have been in use and continued development for more than 10 years. Most recently, a system was utilized in an investigation of the geologic controls on shallow gas distribution in a shallow-water area off the coast of Texas (Meckel and Mulcahy, 2016). This latter study represents one of the first documentations of the use of a UHR3D system in a very shallow-water environment.

Technology

Keeping in the spirit of this special section's theme, we will consider the entire 3D array to be the sensor in the following discussion. This is perfectly appropriate given the array's uniqueness. While this UHR3D system employs solid streamers that incorporate state-of-the-art clustered polyvinylidene fluoride (PVDF) cylindrical hydrophones, this is not what makes UHR3D seismic systems new or unique. The novel aspect is the deployment, geometry, and positioning of the hydrophones.

A UHR3D seismic system, in essence, is a distilled 3D seismic array that provides only near-offset data, but with very high sampling rates, very tight inline and crossline group spacing, and precise positioning (Brookshire et al., 2015). The key innovation of UHR3D seismic systems is the ability to deploy multiple streamers with a very short crossline spacing (as little as 6.25 m). This may be accomplished in different ways, but in the case of our example system mentioned earlier, a single cross-cable allows for up to 24 streamers to be deployed from only four winches instead of 24 individual winches (Figure 1). This has an enormous impact on cost, allowing many short streamers to be towed from a relatively small vessel. And while there are many benefits to towing long streamers, such as amplitude variation with offset (AVO), there are also measureable benefits to towing short streamers, given the right application. Short streamers mean shorter turn times (on the order of 20 to 30 minutes), greater operational efficiency, and increased maneuverability (e.g., close approach to infrastructure) than would be expected during standard high-resolution 2D streamer (1200-plus m) acquisition. Also, in the case of UHR3D seismic methods, shorter streamers allow smaller crossline spacing, fewer aliasing artifacts, and, most importantly, higher resolution.

Horizontal resolution is determined by the geometry of the array, the frequency content of the recorded signal (which impacts

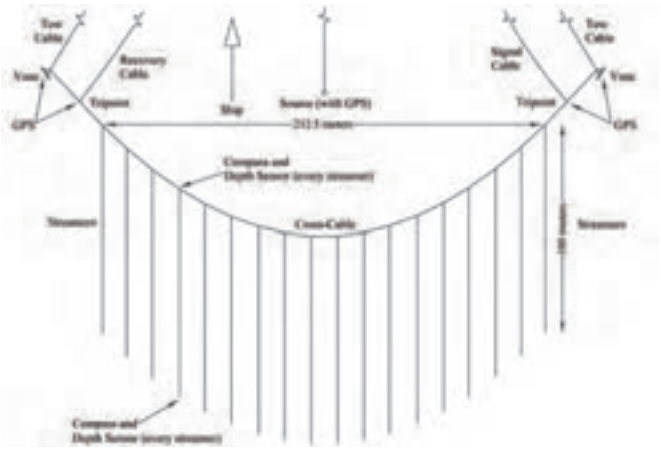

Figure 1. Scaled towing schematic for an 18-streamer UHR3D array. Modified from Brookshire et al., 2015.

[1]NCS Subsea Inc.
[2]Geometrics Inc.

http://dx.doi.org/10.1190/tle35070594.1.

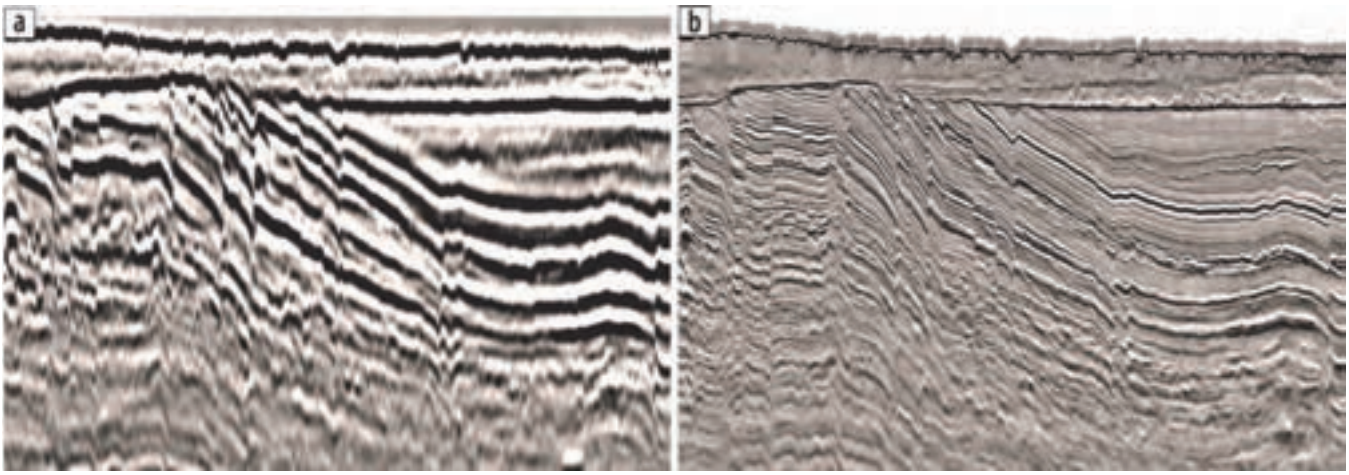

Figure 2. (a) Conventionally acquired and processed exploration 3D seismic data. (b) UHR3D data from the same location. Data courtesy of TGS.

spatial aliasing), and the quality of the positioning data. Given that the largest natural bin size commonly employed in UHR3D acquisition is 3.125 m × 6.25 m, neither bin size nor spatial aliasing impose a significant limitation on horizontal resolution. The major limiting factor here is the quality of the positioning data, which requires some special consideration given the scale of a typical UHR3D array.

Typical positioning strategies that involve multiple compass birds, acoustics, head buoys, tail buoys, etc., are difficult to employ given the use of a cross-cable and the close proximity of the streamers. In consideration of this, the patented NavPoint Trawler system (patents US8069006 B1, US8086408 B1, and US8332174 B1) was designed specifically for use with UHR3D systems, and employs redundant differential global positioning system (dGPS) units at the ends of the cross-cable as absolute positioning references. These observations are combined with those from (three-axis) compasses and depth sensors on the cross-cable near the head of each streamer, and compasses and depth sensors located at each streamer's tail. These data are input to an iterative least-squares algorithm at every shot to produce a network-adjusted position for each receiver group in the array. The positioning data are utilized in real time to populate a binning display for use in steering and monitoring coverage. The data are further refined by incorporating first breaks (ranges derived from source to receiver direct arrival times), which introduce many more degrees of freedom into the network adjustment. First breaks can be applied in near real time to facilitate the identification and mitigation of positioning errors caused by compass biases, and more extensively in post processing. This results in a more robust solution set and, therefore, a higher degree of confidence in the accuracy of the data.

In regard to vertical resolution and given the numerous options for generating a broadband seismic signal, such as air guns, sparkers, triple-plate boomers, etc., the seismic source hardware is not a limiting factor. A source of appropriate bandwidth and cycle rate can be chosen on a case-by-case basis. The receiver array and recording system represent the potential bottleneck in regard to recovering a broadband signal. To mitigate this challenge, the streamer and recording system utilize analog-to-digital-converter modules with a high maximum sampling rate of 8000 Hz (sampling interval of ⅛ millisecond). This, when combined with >110 dB common mode rejection and clustered hydrophone groups, allows for the sampling of very-high-frequency wavelets with very little electrical noise. On the other end of the frequency spectrum, the high hydrophone count of the streamer (12 per group) brings the -3 dB point down to around 5 Hz. The solid construction and polymer hydrophone design of the streamer also effectively eliminates bulge waves and other cable-borne noise. In concert, these features allow for the collection of more than six octaves of usable bandwidth. Given the right hardware, a methodical approach to acquisition that provides good sampling/constraint of near-surface statics, and cutting-edge broadband processing, the use of UHR3D seismic data for many things — from exploration to identifying bubbles in the water column — is a reality.

Data comparisons

Even with a sense of scale, it is often difficult to fully appreciate the benefit of resolution that a UHR3D seismic system affords. The best way to illustrate this is by providing comparisons between UHR3D seismic data and conventionally acquired and processed 3D seismic data. Figure 2 represents such a comparison. Of particular note, and beyond the clear step in horizontal and vertical resolution, are the sharp reflectors, subtle stratigraphic character, exceptionally imaged fault planes, and the well-defined seafloor.

Similarly, Figure 3 illustrates the comparison between conventionally acquired and processed 3D data, conventionally acquired 3D data reprocessed for high resolution, and UHR3D data. Here, the conventional data were acquired with 6000 m streamers with 100 m crossline separation and a 12.5 m group interval. Dual sources were employed (at half the streamer separation) to achieve a natural bin size of 6.25 m × 25 m (processing grid at 12.5 m × 18.75 m), and the data were collected with a sampling interval of 2 ms and processed at a sampling interval of 4 ms (Figure 3a). The data were later reprocessed via Clari-Fi at the field-sampling interval of 2 ms (Figure 3b). The UHR3D data were acquired with 25 m streamers with 12.5 m crossline separation and a 3.125 m group interval. The natural bin size is 1.5625 m × 6.25 m, but the data were processed with a bin size of 6.25 m × 4.75 m.

Even with advanced, purposeful processing techniques, the difference between the reprocessed 3D and UHR3D data is stark. The key takeaway here is that no amount of reprocessing can overcome all the shortcomings of acquisition in regard to resolution.

In particular, the limitations imposed by a large sampling interval and crossline receiver spacing cannot be defeated, only mitigated.

So, what about high-resolution 2D, which has been the staple of geohazard work for decades? Figure 4 illustrates the difference between high-resolution 2D and UHR3D data. Here again, the UHR3D data show the benefits of a higher-frequency content. And, we can rest assured that the 3D data properly comprehend the true nature of the subsurface. The question of what is in or out of plane becomes irrelevant when assessing potential geohazards.

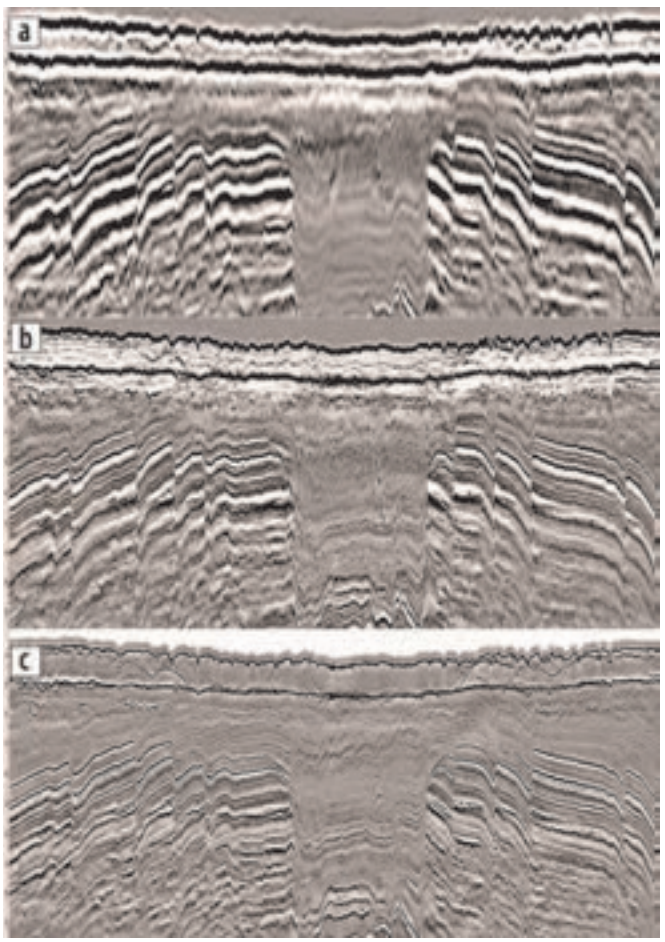

Figure 3. (a) Conventionally acquired and processed exploration 3D seismic data. (b) The same conventionally acquired 3D exploration data reprocessed for high-resolution. (c) UHR3D data from the same location. Data courtesy of TGS.

Case study

The integration of data, such as multibeam echosounder, high-resolution 2D or reprocessed 3D seismic, subbottom profiler, and side-scan sonar, is rewarding in the sense that it presents a technical challenge, and the integrated data can provide a more complete, higher-confidence picture of the seafloor and subsurface. However, those of us who have spent a lot of time integrating different data types know that, with few exceptions, the process is often time consuming and challenging. The purpose of the ongoing study presented here is to use UHR3D seismic data to characterize the seafloor and subsurface expressions of seep features in the GoM over a large area (hundreds of km^2) at very high resolution (on the order of meters). The scope and resolution of these data have allowed us to qualitatively and quantitatively assess a significantly large number of seep features (Brookshire et al., 2016). This is unique among other studies of seep features in the GoM, not only because of the combination of scope and resolution, but because of the comprehensive way in which the seep features can be assessed using a single type of data.

The data were acquired using a UHR3D system composed of 18 × 100 m long streamers with a receiver group spacing of 6.25 m and a cross-line streamer spacing of 12.5 m. Data were collected at the natural bin size of 3.125 × 6.25 m with a shot point spacing of 12.5 m, which yielded four fold of coverage. Sail lines were spaced at 100 m providing two common-midpoint (CMP) lines of overlap between adjacent swaths. A 210 in^3 generator-injector (GI) gun, fired in harmonic mode (~6 bar-m peak-to-peak), was employed. The nominal near offset was held at about 80 m (Brookshire et al., 2015). The data presented here were processed based on the 3D processing flow presented below (Brookshire et al., 2016):

- 20 Hz low-cut filter
- temporal resample to 0.5 ms

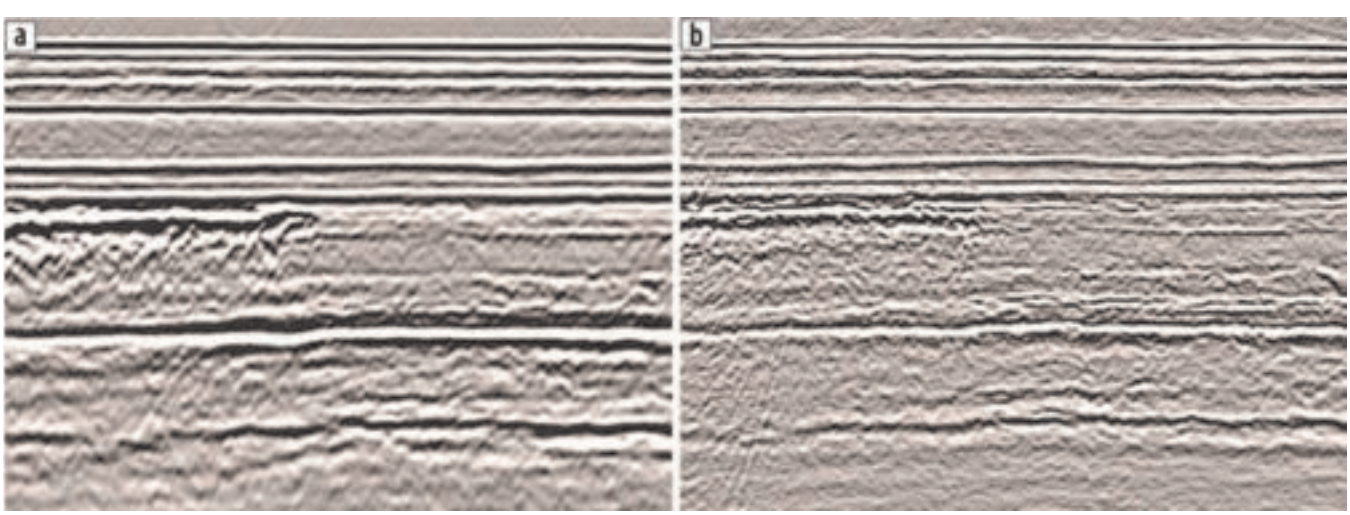

Figure 4. (a) High-resolution 2D data traditionally used for geohazard assessment and well clearance. (b) UHR3D data from the same location. Data courtesy of Statoil.

- statics corrections
- 2D SRME on common channel/shots
- zero-phase operator
- noise attenuation
- regularization
- prestack time migration
- 3D stack
- amplitude balancing

Given the scope of the data set, we decided to employ a top-down strategy in identifying seep features, first focusing on the sediment/water interface. To this end, we carefully picked the seafloor horizon and utilized 3D interpolation tools to develop a detailed seafloor bathymetry, which by virtue of the seismic data also has seafloor amplitude values associated. Seep features were identified based on the apparent seafloor morphologic expression. The Z-component of interpreted seafloor horizon, originally expressed as two-way traveltime, was globally converted to depth using a 1500 m/s conversion factor. The 3D surface was slope-shaded and features were identified collaboratively as mounds, depressions, or complex features with the following criteria: the feature must be closed or semiclosed if on an ambient slope; the feature must demonstrate a slope of 5° or greater.

Following this, each feature was examined in more detail and defined based on the 5° degree slope perimeter. In instances where the 5° slope perimeter was not perfectly continuous (dropping below 5°), a reasonable interpretation of the perimeter was made. All further measurements of width, area, volume, and height were made within this perimeter. Width was measured at the widest point for each feature. Height (negative numbers for depth) was calculated as the difference between the highest and lowest point for each feature. The area of each feature was calculated using Global Mapper software. The cut (positive space) and fill (negative space) volumes for each feature were also calculated using Global Mapper. The cut volume is utilized for mounds, and the fill volume is utilized for depressions. Complex features were not assigned a height or volume due to the relative ambiguity of these measurements resultant from the bathymetric irregularity of these features (Brookshire et al., 2016).

In addition to the seafloor morphology, the water column near the seafloor was assessed for root-mean-square (rms) amplitude anomalies. The automated volume calculation was parameterized to look for the maximum rms amplitude for each trace between 20 ms and 35 ms above the seafloor.

The subsurface expression of each seep feature was reviewed on an individual basis. Seep features exhibiting subsurface bottom simulating reflector (BSR)-like anomalies were noted. BSRs were identified based on coherency, relative amplitude, polarity reversal from the seafloor, and level of bottom simulation (more apparent in some cases than others).

Within the 416 km^2 interpretation area, 52 discrete seep features with clear morphologic expression at the seafloor were identified. An overview map of the identified features is presented in Figure 5. Summary statistics for these features are presented in Table 1. These results reveal that seep features are a common component of the seafloor morphology, comprising around 1% of the seafloor in the interpreted area. This is a conservative estimate because there are subsurface indicators of seepage that are not clearly translated into the seafloor geomorphology.

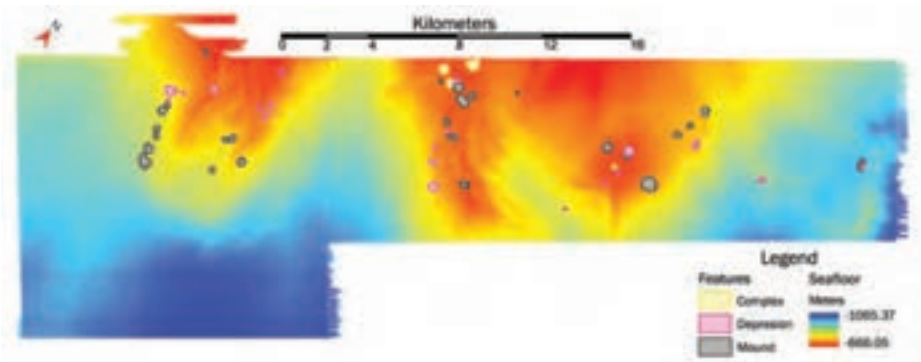

Figure 5. Bathymetry map derived from the UHR3D data with seep feature footprints overlaid. Adapted from Brookshire et al., 2016.

Figure 6 is a three-level representation of the BSR (Figure 6a), seafloor (Figure 6b), and water column amplitudes (Figure 6c) associated with a group of seep features. The associated seismic profile is included and scaled to the horizontal dimensions of the plan view amplitude extractions (Figure 6a1). A shaded 3D bathymetric

Table 1. Summary statistics for the 52 identified seep features. Adapted from Brookshire et al., 2016.

Feature type	Number	Average width (m)	Average height (m)	Average volume (m^3)	Average footprint area (km^2)	Total footprint area (km^2)	Total footprint area percentage of interpreted area (416.290 km^2)	Number with apparent BSR-like anomaly
Mound	28	337	16	313392	0.084	2.353	0.565	19
Depression	20	277	-14	268586	0.054	1.089	0.262	2
Complex	3	425	n/a	n/a	0.129	0.297	0.071	1
Incomplete	1	n/a	n/a	n/a	n/a	0.218	0.052	n/a
TOTAL	52	n/a	n/a	n/a	n/a	3.957	0.951	n/a

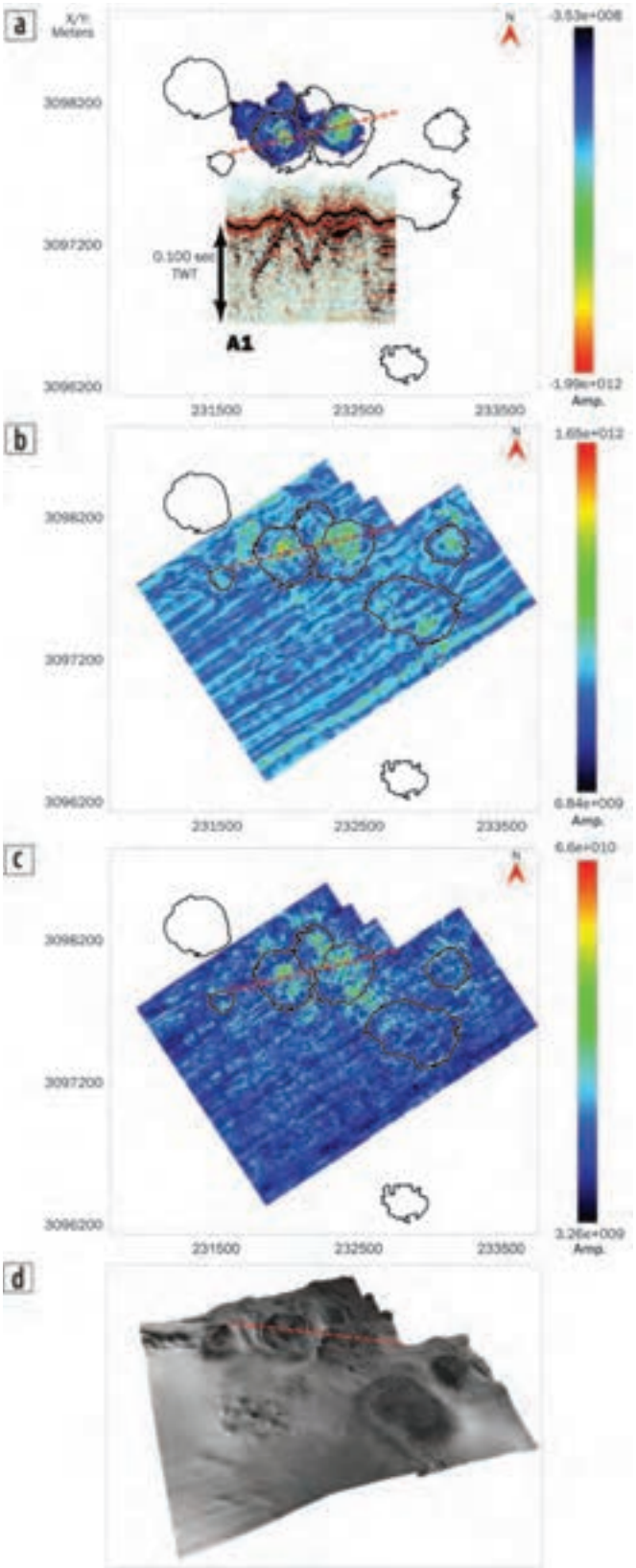

Figure 6. (a) Amplitude extraction for the interpreted time horizon corresponding to the free-gas anomaly imaged in the inset profile (a1). The red dotted line represents the position of the profile in relation to the base map. (b) Amplitude extraction for the interpreted seafloor horizon [same area as shown in (a)]. (c) Water column RMS amplitude calculated for the volume between 0.020 sec and 0.035 sec above the seafloor. (d) Optimally rotated 3D surface illustrating relative relief of the seep features. Adapted from Brookshire et al., 2016.

surface is also included in illustration of the relative relief of the features (Figure 6d). These amplitude extractions reveal a correlation between subsurface BSR amplitude maxima, reflectivity at the seafloor (mineralization?), and noise in the water column — possibly representing bubbles (MacDonald et al., 1994; Roberts, 2001). The latter conclusion, though unconfirmed, is feasible as the authors have received information from industry sources confirming that autonomous underwater vehicle (AUV)-acquired side-scan sonar data from the area contain water column anomalies consistent with bubbles in the water column.

Figure 7 shows one of the clearest examples of a BSR imaged in the data set. This BSR simulates the seafloor reasonably well, in spite of the complex bathymetry of the mound, and displays increased dips, most notable on the flanks, relative to the seafloor. The pull-up of the BSR relative to the dip of the overlying seafloor implies an underestimation of the velocity between the seafloor and BSR, and, hence, the presence of gas hydrates (Scholl and Hart, 1993; Milkov and Sassen, 2000). Finally, Figure 8 completes the story as a representative example of the shallow gas accumulations and migration pathways feeding a seep feature identified in the dataset. The knowledge of increased fluid flow along the flanks of salt features is not new, but the level of clarity in imaging afforded by UHR3D methods is more than novel; it changes expectations by revealing what is possible with a purpose-designed system.

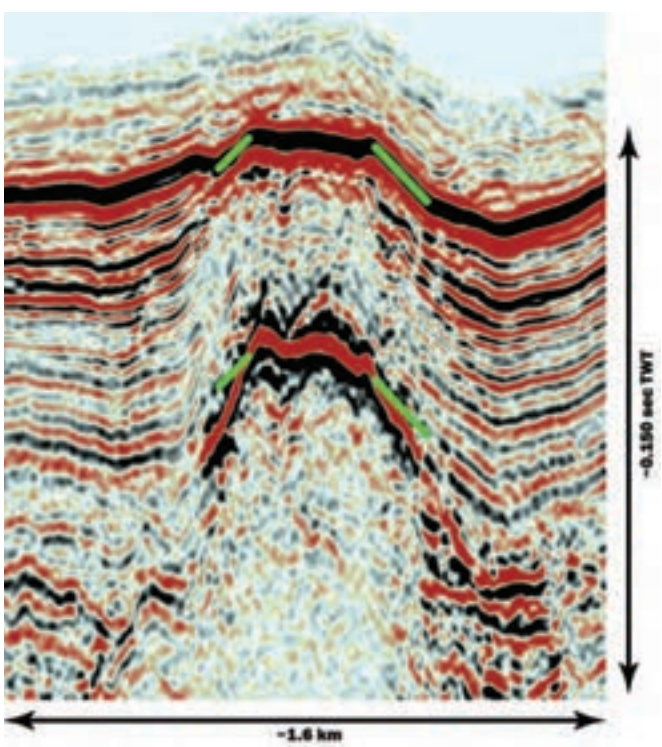

Figure 7. Close-up of a BSR with (green) lines indicating the dip at the immediately overlying seafloor superimposed. Note the increased dip of the BSR relative to the seafloor (pull-up), which the authors interpret to be a sign of underestimated velocities between the seafloor and BSR, indicative of the presence of gas hydrate. Adapted from Brookshire et al., 2016.

Conclusions

UHR3D technology represents a significant advancement in the field of marine seismic data acquisition. In the case of UHR3D, it is not the sensors themselves that are new or unique, but rather the system as a whole, and the methodologies used to deploy and position the sensors. From concept to construction, UHR3D seismic systems are developed and refined toward the application of collecting high-resolution seismic data for shallow exploration and geohazard investigation. With a price tag very similar to 2D high-resolution seismic acquisition and/or AUV acquisition, there is little financial risk in embracing a UHR3D methodology rather than a composite of other acquisition strategies. The amount of time saved in terms of data integration is significant unto itself. As we hopefully move toward a stronger energy economy, ongoing applications of UHR3D technology will undoubtedly lay the foundation for future high-resolution geophysical investigations and further the development of the system to address even more complex applications such as 4D and life-of-field studies. TLE

Corresponding author: craig@geometrics.com

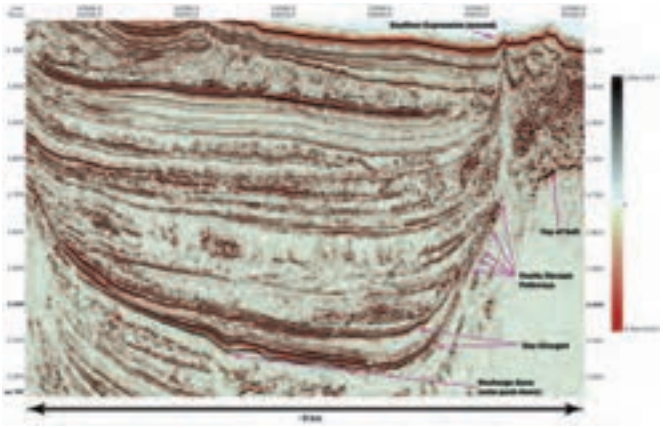

Figure 8. Profile from the 3D PSTM seismic volume illustrating the possible gas migration pathways in the shallow subsurface. Adapted from Brookshire et al., 2016.

Acknowledgments

The authors would like to thank the SAFE-BAND group (NCS SubSea, Geotrace, and Spec Partners), TGS, and Statoil for providing data presented in this article. We would also like to thank Clayton Mills and Larry Scott for providing thoughtful comments on the manuscript.

References

Brookshire, B. N. Jr., F. P. Landers, and J. A. Stein, 2015, Applicability of ultra-high-resolution 3D seismic data for geohazard identification at mid-slope depths in the Gulf of Mexico: Initial results: Underwater Technology, **32**, no. 4, 271–278, http://dx.doi.org/10.3723/ut.32.271.

Brookshire, B. N. Jr., B. A. Mattox, A. E. Parish, and A. G. Burks, 2016, Ultrahigh-resolution 3-dimensional seismic imaging of seeps from the continental slope of the northern Gulf of Mexico: Subsurface, seafloor and into the water column: NCS SubSea, http://www.ncs-subsea.com/UHR3D%20Seismic%20Imaging%20of%20Seeps%20GOM.dmx, accessed 3 June 2016.

Eriksen, F. N., M. Assad, O. K. Eriksen, H. H. Stokke, and S. Planke, 2014, HiRes P-Cable 3D data for shallow reservoir mapping and geohazard predictions — Case examples from the Barents Sea: Paper read at Near Surface Geoscience 2014 — First Applied Shallow Marine Geophysics Conference.

Hill, A. W., A. Arogunmati, G. A. Wood, D. Attoe, M. Fiske, A. Dingler, J. A. Dingler, M. Hobson, A. Robertshaw, C. Allinson, E. Kjos, M. Higson, T. Manning, K. Kassarie, and S. M. Lewis, 2015, Slicing and dicing HR seismic acquisition: Varied approaches to delivery of high-resolution 3D seismic data volumes for drilling-hazard studies: The Leading Edge, **34**, no. 4, 380–388, http://dx.doi.org/10.1190/tle34040380.1.

Kluesner, J. W., and D. S. Brothers, 2016, Seismic attribute detection of faults and fluid pathways within an active strike-slip shear zone: New insights from high-resolution 3D P-Cable™ seismic data along the Hosgri Fault, offshore California: Interpretation, **4**, no. 1, SB131–SB148, http://dx.doi.org/10.1190/INT-2015-0143.1.

MacDonald, I., N. Guinasso Jr., R. Sassen, J. Brooks, L. Lee, and K. Scott, 1994, Gas hydrate that breaches the sea floor on the continental slope of the Gulf of Mexico: Geology, **22**, no. 8, 699–702, http://dx.doi.org/10.1130/0091-7613(1994)022<0699:GHTBTS>2.3.CO;2.

Meckel, T. A., and F. J. Mulcahy, 2016, Use of novel high-resolution 3D marine seismic technology to evaluate Quaternary fluvial valley development and geologic controls on shallow gas distribution, inner shelf, Gulf of Mexico: Interpretation, **4**, no. 1, SC35–SC49, http://dx.doi.org/10.1190/INT-2015-0092.1.

Milkov, A. V., and R. Sassen, 2000, Thickness of the gas hydrate stability zone, Gulf of Mexico continental slope: Marine and Petroleum Geology, **17**, no. 9, 981–991, http://dx.doi.org/10.1016/S0264-8172(00)00051-9.

Roberts, H. H., 2001, Fluid and Gas Expulsion on the Northern Gulf of Mexico Continental Slope: Mud-prone to mineral-prone responses, in Paull C. K. and W. P. Dillon (eds.), Natural gas hydrates: Occurrences, distribution, and detection: AGU Geophysical Monograph Series, **24**, 145–161.

Scholl, D. W., and P. E. Hart, 1993, Velocity and amplitude structures on seismic-reflection profiles — Possible massive gas-hydrate deposits and underlying gas accumulations in the Bering Sea Basin, in Howell, D. G., ed., The future of energy gases: U. S. Geological Survey Professional Paper, **1570**, 331–352.